PHYSICS OF FLUIDS **27**, 052101 (2015)

# A rivulet of a power-law fluid with constant contact angle draining down a slowly varying substrate

F. H. H. Al Mukahal,[a] B. R. Duffy,[b] and S. K. Wilson[c]
*Department of Mathematics and Statistics, University of Strathclyde, 26 Richmond Street, Glasgow G1 1XH, United Kingdom*

(Received 14 November 2014; accepted 8 April 2015; published online 6 May 2015)

Locally unidirectional steady gravity-driven flow of a thin rivulet of a power-law fluid with prescribed volume flux down a locally planar substrate is considered. First, the solution for unidirectional flow of a uniform rivulet down a planar substrate is obtained, and then it is used to obtain the solution for a slowly varying rivulet with prescribed constant (nonzero) contact angle down a slowly varying substrate, specifically flow in the azimuthal direction around the outside of a large horizontal circular cylinder. The solution is shown to depend strongly on the value of the power-law index of the fluid. For example, a rivulet of strongly shear-thinning fluid "self-channels" its flow down a narrow central channel between two "levées" of slowly moving fluid that form at its sides, and in the central channel there is a "plug-like" flow except in a boundary layer near the substrate. On the other hand, in a rivulet of a strongly shear-thickening fluid the velocity profile is linear except in a boundary layer near the free surface. Another notable qualitative departure from Newtonian behaviour is that, whereas the mass of a rivulet of a Newtonian or a shear-thinning fluid is theoretically infinite, the mass of a rivulet of a shear-thickening fluid is finite. © *2015 AIP Publishing LLC.* [http://dx.doi.org/10.1063/1.4919342]

## I. INTRODUCTION

Rivulet flow of a viscous fluid is a problem of enduring theoretical and experimental interest, not least because it occurs in a wide range of practical and industrial situations, including condensers and heat exchangers,[1] geophysical flows of ice, lava, and mud,[2] rain-wind-induced vibrations of cable-stayed bridges,[3,4] two-phase flow in narrow capillaries,[5] and even rivulets of rain water draining down a window pane.

The pioneering studies of the steady locally rectilinear flow of a locally uniform rivulet of a Newtonian fluid down a locally planar substrate were performed by Towell and Rothfeld,[6] Allen and Biggin,[7] and Duffy and Moffatt.[8] Subsequently, this work has been extended to include, for example, non-planar substrates,[9–12] thermocapillary effects,[13] thermoviscosity effects,[14] and the presence of an external airflow.[15–18] Recently, the pinning, de-pinning, and re-pinning of a rivulet have also been studied.[19] In addition, similarity solutions have been obtained and analysed for steady[20,21] and unsteady[22] flows of non-uniform rivulets. There has also been considerable work on the stability of rivulet flow,[23–29] on waves on rivulets,[30–33] and on rivulet braiding and meandering.[34–38]

However, despite the widespread occurrence of non-Newtonian rheology in many of the practical occurrences of rivulet flow, there has been surprisingly little theoretical work on rivulet flow of non-Newtonian fluids. Rare exceptions include the work by Rosenblat[39] on rivulet flow of a viscoelastic fluid, and that by Wilson, Duffy, and Ross[40] on rivulet flow of viscoplastic material. In addition, similarity solutions have been obtained and analysed for steady[41,42] and unsteady[43] flows of non-uniform rivulets of a power-law fluid.

[a]Email: fatemah.al-mukahal@strath.ac.uk
[b]Email: b.r.duffy@strath.ac.uk
[c]Author to whom correspondence should be addressed. Electronic mail: s.k.wilson@strath.ac.uk

 

The present work begins to rectify this lack of understanding of non-Newtonian rivulet flow by analysing the locally unidirectional steady gravity-driven flow of a thin rivulet of a power-law fluid with prescribed volume flux down a locally planar substrate. First, we obtain the solution for unidirectional flow of a uniform rivulet down a planar substrate, and then we use it to obtain the solution for a slowly varying rivulet with prescribed constant (nonzero) contact angle down a slowly varying substrate, specifically flow in the azimuthal direction around the outside of a large horizontal circular cylinder. While the shortcomings of the power-law model (particularly the large viscosity at low shear rate in the shear-thinning case and the small viscosity at low shear rate in the shear-thickening case) are, of course, well known (see, for example, Myers[44]), valuable insight can still be gained from its use. In particular, the present results provide a benchmark for the study of rivulet flow of more realistic non-Newtonian fluids.

## II. A POWER-LAW FLUID

The mass-conservation and momentum-balance equations for an incompressible fluid of density $\rho$ take the forms

$$\nabla \cdot \mathbf{u} = 0, \qquad \rho \frac{D\mathbf{u}}{Dt} = -\nabla p + \rho \mathbf{g} + \nabla \cdot \boldsymbol{\sigma}, \tag{1}$$

where $\mathbf{u}$ and $p$ are the velocity and pressure, respectively, $\mathbf{g}$ denotes acceleration due to gravity, $t$ denotes time, and $\boldsymbol{\sigma}$ is the extra-stress tensor (that is, the part of the stress other than the pressure), which is related to kinematic (and perhaps other) variables via constitutive relations for the particular fluid under study (see, for example, Barnes, Hutton, and Walters[45]).

A generalised Newtonian fluid is one for which the viscosity varies with the shear rate, so that the relation between extra stress and shear rate is nonlinear. In the present work, we shall be concerned with the simplest such fluid, namely, a power-law fluid, for which the viscosity is a power of the shear rate, so that the constitutive relation takes the form

$$\boldsymbol{\sigma} = 2\mu(q)\mathbf{e}, \qquad \mu(q) = \mu_N q^{N-1}, \tag{2}$$

where $\mathbf{e}$ is the rate-of-strain tensor, given by

$$\mathbf{e} = \frac{1}{2}\left(\nabla \mathbf{u} + (\nabla \mathbf{u})^{\mathrm{T}}\right), \tag{3}$$

$q$ is the shear rate, given by $q = \left(2\,\mathrm{tr}\left(\mathbf{e}^2\right)\right)^{1/2}$, and the power-law index $N$ and the consistency parameter $\mu_N$ are constants; note that the dimensions of $\mu_N$ depend on $N$. The measure of the extra stress, $\tau$, defined by $\tau = \left(\frac{1}{2}\mathrm{tr}\left(\boldsymbol{\sigma}^2\right)\right)^{1/2}$ takes the form $\tau = \mu(q)q = \mu_N q^N$. In practice, $N$ is usually found to lie between 0.1 and 1, although values outside this range do occur, and so in order to investigate the full range of possible behaviour in the present work we shall allow $N$ to take any positive value. A power-law fluid is shear thinning (that is, $\mu$ decreases with $q$) when $0 < N < 1$ and is shear thickening (that is, $\mu$ increases with $q$) when $N > 1$; when $N = 1$, the special case of a Newtonian fluid with constant viscosity is recovered.

## III. RIVULET FLOW DOWN A PLANAR SUBSTRATE

### A. Formulation

First, we consider unidirectional steady gravity-driven flow of a thin uniform rivulet of a power-law fluid with prescribed volume flux down a planar substrate inclined at an angle $\alpha$ to the horizontal, as shown in Fig. 1. The case $0 \le \alpha < \pi/2$ corresponds to flow down the upper side of the substrate (a sessile rivulet), and the case $\pi/2 < \alpha \le \pi$ corresponds to flow down the lower side of the substrate (a pendent rivulet); the special case $\alpha = \pi/2$ corresponds to flow down a vertical substrate and will be considered in detail in Subsection III C. Referred to the Cartesian coordinates $Oxyz$ shown in Fig. 1, the substrate is at $z = 0$, and we denote the cross-sectional free surface profile of the rivulet by $z = h(y)$; also we denote the semi-width of the rivulet by $a$, the fluid

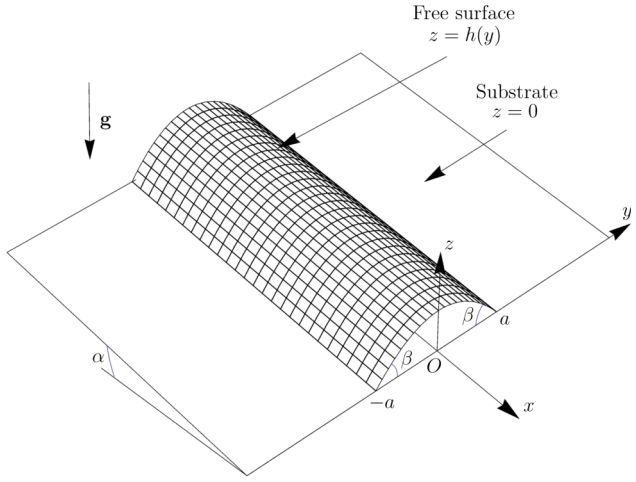


FIG. 1. Sketch of the unidirectional steady gravity-driven flow of a thin uniform rivulet of a power-law fluid of prescribed volume flux down a planar substrate inclined at an angle $\alpha$ to the horizontal.

occupying $-a \le y \le a$. We consider the situation in which the contact angle of the fluid, $\beta$ ($> 0$), has a prescribed (nonzero) value, but the semi-width $a$ is unknown and is to be determined as part of the solution. Not only is this flow of interest in its own right but it also forms the basis for studying the flow of a slowly varying rivulet with constant contact angle down a slowly varying substrate described in Sec. IV.

With a velocity of the form $\mathbf{u} = u(y,z)\mathbf{i}$, the shear rate is $q = \left(u_y^2 + u_z^2\right)^{1/2}$, but since the rivulet is thin we have $q = |u_z|$ to the usual accuracy of thin-film theory; moreover, since $u_z \ge 0$ for the type of flow under consideration, we have $q = u_z$. Therefore, (1)–(3) reduce to

$$0 = -p_x + \rho g \sin\alpha + \mu_N (u_z^N)_z, \qquad 0 = -p_y, \qquad 0 = -p_z - \rho g \cos\alpha, \tag{4}$$

to be integrated subject to the boundary conditions

$$u = 0 \text{ on } z = 0, \qquad u_z = 0 \text{ and } p = p_a - \gamma h'' \text{ on } z = h, \tag{5}$$

where $p_a$ denotes atmospheric pressure, $\gamma$ denotes the coefficient of surface tension of the fluid, and a prime denotes differentiation with respect to $y$. In addition, $h$ satisfies the contact-line conditions

$$h = 0 \text{ and } h' = \mp\beta \text{ at } y = \pm a. \tag{6}$$

The volume flux of fluid along the rivulet, $Q$, is given by

$$Q = \int_{-a}^{a} \int_{0}^{h} u \, \mathrm{d}z \, \mathrm{d}y, \tag{7}$$

which will be taken to have a prescribed value $Q = \bar{Q}$.

We non-dimensionalise and scale the variables appropriately by writing

$$\begin{aligned} &y = \ell y^*, \quad a = \ell a^*, \quad z = \beta \ell z^*, \quad h = \beta \ell h^*, \quad u = U u^*, \quad p = p_a + \rho g \beta \ell p^*, \\ &Q = \beta \ell^2 U Q^*, \quad q = \frac{U}{\beta \ell} q^*, \quad \mu = \bar{\mu} \mu^*, \quad \tau = \rho g \beta \ell \tau^*, \end{aligned} \tag{8}$$

where $\ell = (\gamma/\rho g)^{1/2}$ is the capillary length, $U = (\rho g \beta^{N+1} \ell^{N+1}/\mu_N)^{1/N}$ is an appropriate velocity scale, and $\bar{\mu} = \mu_N (U/\beta\ell)^{N-1}$ is an appropriate viscosity scale. Note that the scales $U$ and $\bar{\mu}$ depend on $\mu_N$ and $N$, and that the scaled contact angle is $\beta^* \equiv 1$ and the scaled viscosity is $\mu^* = q^{*N-1}$. From now on, we use non-dimensional quantities (omitting the stars, for clarity).

### B. Solution

From $(4)_3$ and (5) the solution for $p$ is

$$p = \cos\alpha(h - z) - h'', \tag{9}$$

and then $(4)_2$ gives

$$(h'' - \cos\alpha\, h)' = 0, \tag{10}$$

representing a transverse balance between gravity and surface-tension effects. Since (10) does not depend on viscous effects, the general form of solution for $h$ will be independent of $N$; in particular, it will be the same as that for a Newtonian fluid (and indeed for any generalised Newtonian fluid).

The solution of (6) and (10) for $h$ is

$$h = \begin{cases} \dfrac{\cosh ma - \cosh my}{m \sinh ma} & \text{if } 0 \le \alpha < \dfrac{\pi}{2}, \\ \dfrac{a^2 - y^2}{2a} & \text{if } \alpha = \dfrac{\pi}{2}, \\ \dfrac{\cos my - \cos ma}{m \sin ma} & \text{if } \dfrac{\pi}{2} < \alpha \le \pi, \end{cases} \tag{11}$$

where we have introduced the notation $m = \sqrt{|\cos\alpha|}$. We note that the rivulet is symmetric about its centreline $y = 0$, and so its maximum thickness $h_\mathrm{m} = h(0)$ occurs at $y = 0$ and is given by

$$h_\mathrm{m} = \begin{cases} \dfrac{1}{m}\tanh\dfrac{ma}{2} & \text{if } 0 \le \alpha < \dfrac{\pi}{2}, \\ \dfrac{a}{2} & \text{if } \alpha = \dfrac{\pi}{2}, \\ \dfrac{1}{m}\tan\dfrac{ma}{2} & \text{if } \dfrac{\pi}{2} < \alpha \le \pi. \end{cases} \tag{12}$$

It may be shown that, whereas for $0 \le \alpha \le \pi/2$ the solution (11) is valid for any $ma \ge 0$, for $\pi/2 < \alpha \le \pi$ it is physically realisable (specifically, $h \ge 0$ for $-a \le y \le a$) only if $ma < \pi$. As yet, the semi-width $a$ in (11) is unknown.

From $(4)_1$ and (5) the solution for $u$ is

$$u = \frac{N}{N+1}(\sin\alpha)^{\frac{1}{N}}\left(h^{\frac{N+1}{N}} - (h - z)^{\frac{N+1}{N}}\right), \tag{13}$$

representing a longitudinal balance between gravitational and viscous effects. The maximum velocity, $u_\mathrm{max}$, given by

$$u_\mathrm{max} = \frac{N}{N+1}\left(\sin\alpha\, h_\mathrm{m}^{N+1}\right)^{\frac{1}{N}}, \tag{14}$$

occurs at the apex of the rivulet, i.e., at $y = 0$, $z = h_\mathrm{m}$. The shear rate $q$, viscosity $\mu = q^{N-1}$, and shear stress $\tau = \mu q = q^N$ vary across the rivulet and are given by

$$q = [\sin\alpha\,(h - z)]^{\frac{1}{N}}, \qquad \mu = [\sin\alpha\,(h - z)]^{\frac{N-1}{N}}, \qquad \tau = \sin\alpha\,(h - z), \tag{15}$$

respectively. In particular, in the shear-thickening case ($N > 1$), the viscosity $\mu$ decreases monotonically from its value $(\sin\alpha\, h)^{(N-1)/N}$ at the substrate $z = 0$ to zero at the free surface $z = h$, whereas in the shear-thinning case ($N < 1$) it increases monotonically from $(\sin\alpha\, h)^{(N-1)/N}$ at $z = 0$ and becomes infinite at $z = h$. Despite the shortcomings associated with the power-law model (namely, a zero or infinite viscosity at the free surface), the other features of the flow are well behaved; in particular, the velocity $u$, shear rate $q$, and shear stress $\tau$ are finite everywhere (the latter being linear in $z$, as required by the balance of momentum in the $x$ direction).

From (7) and (13) the flux of fluid along the rivulet, $Q$, is

$$Q = \frac{N}{2N+1}(\sin\alpha)^{\frac{1}{N}}\int_{-a}^{a} h^{\frac{2N+1}{N}}\,\mathrm{d}y. \tag{16}$$

Performing the quadrature here, with $h$ given by (11), we find that $Q$ is given by

$$Q = \frac{1}{9}\left(\frac{\sin\alpha}{m^{3N+1}}\right)^{\frac{1}{N}} f_N(ma), \tag{17}$$

where the function $f_N(ma)$ is defined by

$$f_N(ma) = \lambda_N \times \begin{cases} {}_2F_1\left(\frac{1}{2}, \frac{3N+1}{N}; \frac{7N+2}{2N}; \tanh^2\frac{ma}{2}\right)\tanh^{\frac{3N+1}{N}}\frac{ma}{2} & \text{if } 0 \le \alpha < \frac{\pi}{2}, \\ \left(\frac{ma}{2}\right)^{\frac{3N+1}{N}} & \text{if } \alpha = \frac{\pi}{2}, \\ {}_2F_1\left(\frac{1}{2}, \frac{3N+1}{N}; \frac{7N+2}{2N}; -\tan^2\frac{ma}{2}\right)\tan^{\frac{3N+1}{N}}\frac{ma}{2} & \text{if } \frac{\pi}{2} < \alpha \le \pi, \end{cases} \tag{18}$$

in which ${}_2F_1$ denotes the hypergeometric function, and where we have introduced $\lambda_N$ defined by

$$\lambda_N = \frac{18\sqrt{\pi}\,\Gamma\left(\frac{2N+1}{N}\right)}{\Gamma\left(\frac{7N+2}{2N}\right)} = 36\,\mathrm{B}\left(\frac{3}{2}, \frac{2N+1}{N}\right), \tag{19}$$

where $\Gamma$ and B denote the Gamma and Beta functions, respectively. To complete the solution, we must solve (17) with $Q = \bar{Q}$ to obtain the semi-width $a$; this depends on the form of $f_N(ma)$ in (18), and therefore also on the form of $\lambda_N$ in (19).

Figure 2 shows a plot of $\lambda_N$ as a function of $N$, illustrating that $\lambda_N$ increases monotonically with $N$, satisfying

$$\lambda_N = 18\sqrt{\pi}N^{3/2} + O(N^{5/2}) \to 0^+ \quad \text{as} \quad N \to 0^+, \tag{20}$$

$$\lambda_N = \frac{48}{5} - \frac{16}{25}(31 - 15\log 4)\,N^{-1} + O(N^{-2}) \to \frac{48}{5}^- \quad \text{as} \quad N \to \infty, \tag{21}$$

and taking the value $192/35 \simeq 5.485\,71$ at $N = 1$.

Figure 3 shows plots of $f_N(ma)$ as a function of $ma$ in the cases (a) $0 \le \alpha < \pi/2$ and (b) $\alpha = \pi/2$, and as a function of $ma/\pi$ ($0 \le ma/\pi \le 1$) in the case (c) $\pi/2 < \alpha \le \pi$, for a range of values of $N$. Figure 3 illustrates that in all cases $f_N(ma)$ increases monotonically with $ma$, and, in particular,

$$f_N(ma) \sim \lambda_N\left(\frac{ma}{2}\right)^{\frac{3N+1}{N}} = O\left((ma)^{\frac{3N+1}{N}}\right) \to 0^+ \tag{22}$$

in the limit $ma \to 0^+$,

$$f_N(ma) \sim \frac{18N}{2N+1}ma = O(ma) \to \infty \tag{23}$$

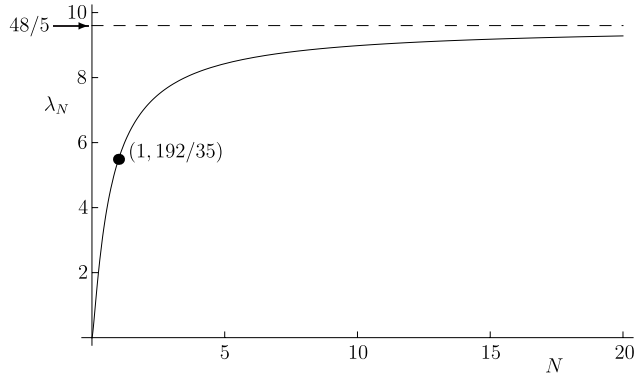


FIG. 2. Plot of $\lambda_N$ defined in (19) as a function of $N$, together with its asymptotic value 48/5 in the limit $N \to \infty$. The dot denotes the Newtonian value 192/35 at $N = 1$.

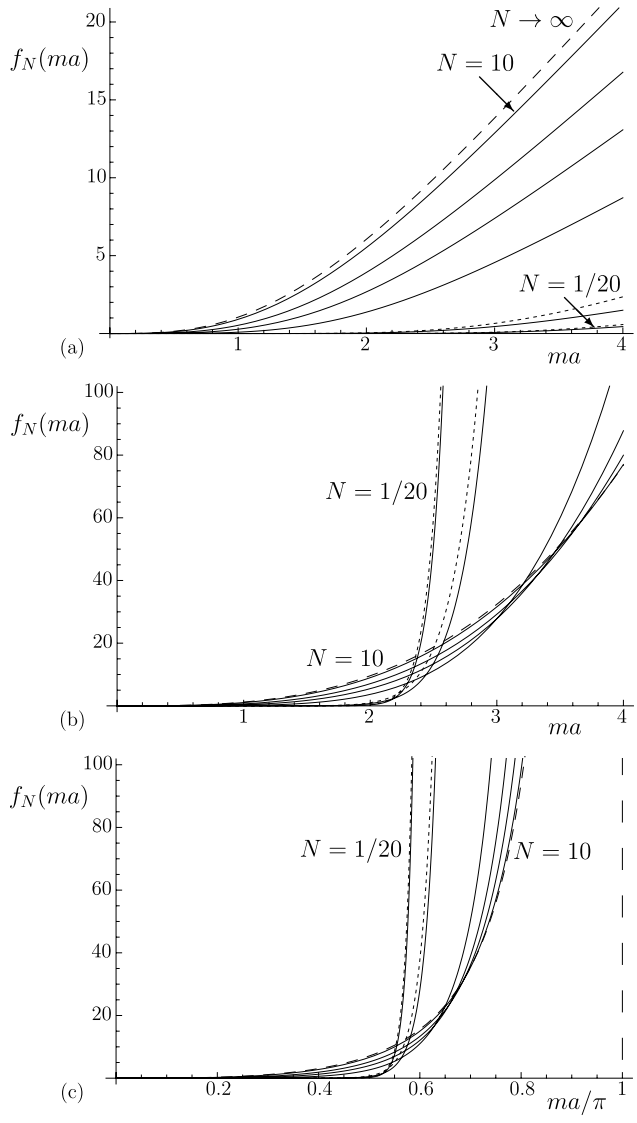


FIG. 3. Plots of $f_N(ma)$ defined in (18) as a function of $ma$ in the cases (a) $0 \le \alpha < \pi/2$ and (b) $\alpha = \pi/2$, and as a function of $ma/\pi$ ($0 \le ma/\pi \le 1$) in the case (c) $\pi/2 < \alpha \le \pi$, for $N = 1/20$, $1/10$, $1/2$, 1, 2, and 10. The dotted lines show the leading-order asymptotic solution in the limit $N \to 0^+$, $\hat{f}_N$, defined in (26) and plotted for $N = 1/20$ and $N = 1/10$, and the dashed lines show the leading-order asymptotic solution in the limit $N \to \infty$, $f_\infty$, defined in (28). The vertical long-dashed line in (c) marks the maximum value of $ma = \pi$ beyond which there are no physically realisable solutions for $h$.

in the limit $ma \to \infty$ for $0 \le \alpha < \pi/2$, $f_N(ma) = \lambda_N (ma/2)^{(3N+1)/N} = O\left(ma^{(3N+1)/N}\right) \to \infty$ in the limit $ma \to \infty$ for $\alpha = \pi/2$, and

$$f_N(ma) \sim 9\left(\frac{2}{\kappa_N(\pi - ma)}\right)^{\frac{2N+1}{N}} = O\left((\pi - ma)^{-\frac{2N+1}{N}}\right) \to \infty \tag{24}$$

in the limit $ma \to \pi^-$ for $\pi/2 < \alpha \le \pi$, where we have introduced $\kappa_N$ defined by

$$\kappa_N = \left(\frac{(2N+1)\Gamma\left(\frac{3N+1}{N}\right)}{2\sqrt{\pi}N\,\Gamma\left(\frac{5N+2}{2N}\right)}\right)^{\frac{N}{2N+1}} = \left[\frac{2N}{2N+1}\,\mathrm{B}\left(\frac{1}{2}, \frac{5N+2}{2N}\right)\right]^{-\frac{N}{2N+1}}. \tag{25}$$

We conclude that (17) has a solution $a$ for any prescribed $N$, $\alpha$, and $\bar{Q}$, and that this solution is unique. [In fact, the function $f_N(ma)$ given in $(18)_3$ for $\pi/2 < \alpha \leq \pi$ has infinitely many branches in $ma \geq 0$; however, since only the branch in $0 \leq ma \leq \pi$ leads to physically realisable solutions for $h$, we shall ignore the branches beyond $ma = \pi$.] The transcendental nature of (17) means that, in general, it must be solved numerically for $a$.

Figure 3 also shows that when $0 \leq \alpha < \pi/2$, $f_N(ma)$ is an increasing function of $N$ for all $ma$, but when $\pi/2 \leq \alpha \leq \pi$ it is an increasing function of $N$ for sufficiently small values of $ma$ but a decreasing function of $N$ for sufficiently large values of $ma$; therefore the curves for different values of $N$ in Figs. 3(b) and 3(c) (but not those in Fig. 3(a)) cross each other.

For future reference, we note that in the limit $N \to 0^+$, we have $f_N(ma) \sim \hat{f}_N(ma)$, where we have defined

$$\hat{f}_N(ma) = 18\sqrt{\pi}N^{\frac{3}{2}} \times \begin{cases} \sinh\dfrac{ma}{2}\tanh^{\frac{2N+1}{N}}\dfrac{ma}{2} & \text{if } 0 \leq \alpha < \dfrac{\pi}{2}, \\ \left(\dfrac{ma}{2}\right)^{\frac{3N+1}{N}} & \text{if } \alpha = \dfrac{\pi}{2}, \\ \sin\dfrac{ma}{2}\tan^{\frac{2N+1}{N}}\dfrac{ma}{2} & \text{if } \dfrac{\pi}{2} < \alpha \leq \pi. \end{cases} \tag{26}$$

For $0 \leq \alpha \leq \pi/2$ the function $\hat{f}_N(ma)$ satisfies $\hat{f}_N(ma) \to 0^+$ as $N \to 0^+$, whereas for $\pi/2 < \alpha \leq \pi$ it satisfies $\hat{f}_N(ma) \to 0^+$ as $N \to 0^+$ when $0 \leq ma \leq \pi/2$, but $\hat{f}_N(ma) \to \infty$ as $N \to 0^+$ when $\pi/2 < ma \leq \pi$. Furthermore, in the limit $N \to \infty$ we have $f_N(ma) \to f_\infty(ma)$ and, from (17),

$$Q \to \frac{f_\infty(ma)}{9m^3}, \tag{27}$$

where we have defined

$$f_\infty(ma) = \begin{cases} \dfrac{9}{2}\left(3ma\coth^2 ma - 3\coth ma - ma\right) & \text{if } 0 \leq \alpha < \dfrac{\pi}{2}, \\ \dfrac{6(ma)^3}{5} & \text{if } \alpha = \dfrac{\pi}{2}, \\ \dfrac{9}{2}\left(3ma\cot^2 ma - 3\cot ma + ma\right) & \text{if } \dfrac{\pi}{2} < \alpha \leq \pi. \end{cases} \tag{28}$$

The functions $\hat{f}_N$ and $f_\infty$ given by (26) and (28) are included in Fig. 3 as dotted and dashed curves, respectively.

In summary, the solutions for the pressure $p$ and velocity $u$ in the steady unidirectional flow of a thin uniform rivulet are given by (9) and (13), respectively, in which the free surface profile $h$ is given by (11), with the semi-width $a$ to be determined from flux condition (17) with $Q = \bar{Q}$ when $N$, $\alpha$, and $\bar{Q}$ are prescribed. In the special case of a Newtonian fluid ($N = 1$), Eqs. (13)–(19) reduce to the solution given by Duffy and Moffatt[8] (albeit presented somewhat differently).

### C. The special case of rivulet flow down a vertical substrate

The special case of rivulet flow down a vertical substrate (that is, the special case $\alpha = \pi/2$) is of particular interest and hence merits further discussion here. In that case, the cross-sectional free surface profile of the rivulet has the simple parabolic form given in (11), and Eqs. (17) and (18) may be solved to give simple explicit solutions for $a$ and hence $h_\mathrm{m}$, namely,

$$a = 2\left(\frac{9\bar{Q}}{\lambda_N}\right)^{\frac{N}{3N+1}}, \quad h_\mathrm{m} = \left(\frac{9\bar{Q}}{\lambda_N}\right)^{\frac{N}{3N+1}}. \tag{29}$$

Figure 4 shows a plot of $a$ given by (29) as a function of $N$ for various values of $\bar{Q}$, and Fig. 5 shows a plot of $a$ as a function of $\bar{Q}$ for various values of $N$. As Figs. 4 and 5 show, for all values of $\bar{Q}$, $a$ satisfies $a \to 2^+$ as $N \to 0^+$ and $a \to (15\bar{Q}/2)^{1/3}$ as $N \to \infty$, and takes the value $a = (105\bar{Q}/4)^{1/4}$ when $N = 1$.

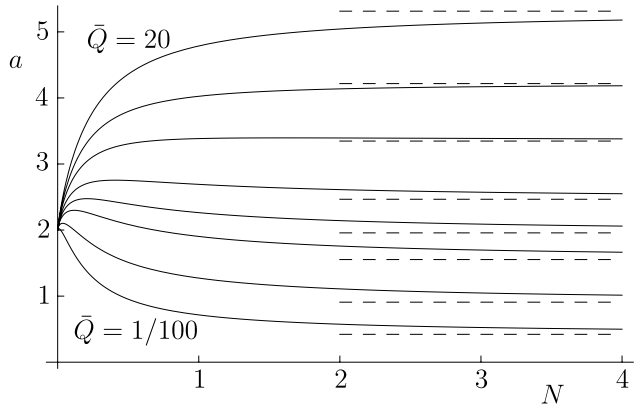


FIG. 4. Plot of the semi-width $a$ given by (29) as a function of $N$ in the special case of a vertical substrate ($\alpha = \pi/2$), for $\bar{Q} = 1/100$, $1/10$, $1/2$, 1, 2, 5, 10, and 20. The dashed lines show the asymptotic solution $a = (15\bar{Q}/2)^{1/3}$ in the limit $N \to \infty$.

As Fig. 4 illustrates, if $\bar{Q}$ is sufficiently small, specifically if $\bar{Q} < \bar{Q}_{\rm m}$, where $\bar{Q}_{\rm m} = 16\exp(\psi(7/2) + \gamma - 1)/15 \simeq 8.212\,48$, in which $\psi(7/2) = \Gamma'(7/2)/\Gamma(7/2) \simeq 1.103\,16$ denotes the Digamma function and $\gamma \simeq 0.577\,22$ denotes Euler's constant, then $a$ first increases with $N$ to a local maximum and thereafter decreases monotonically. The value of $N$ at which this maximum occurs increases with $\bar{Q}$ and becomes infinite when $\bar{Q} = \bar{Q}_{\rm m}$; thus if $\bar{Q}$ is sufficiently large, specifically if $\bar{Q} \geq \bar{Q}_{\rm m}$, then $a$ has no maximum as a function of $N$, and so simply increases monotonically with $N$. As Fig. 4 also shows, whatever the value of $\bar{Q}$ there is only a restricted range of possible values of $a$, and also that if $\bar{Q} < \bar{Q}_{\rm m}$ then it is possible for two rivulets of fluids with different values of $N$, with the same value of $\bar{Q}$, to have the same value of $a$. On the other hand, as Fig. 5 shows, for a given value of $N$, $a$ increases monotonically with $\bar{Q}$; in particular, it is immediately apparent from (29) that $a \to 0^+$ as $\bar{Q} \to 0^+$ and $a \to \infty$ as $\bar{Q} \to \infty$.

Figure 6 shows plots of the velocity profiles $u(y,z)$ given by (13) at different positions $y$ across the rivulet, for (a) a strongly shear-thinning fluid with $N = 1/10$ and (b) a strongly shear-thickening fluid with $N = 10$, with $\bar{Q} = 1$ in each case; from (29) the corresponding semi-widths and maximum thicknesses are $a \simeq 2.422\,64$ and $h_{\rm m} \simeq 1.211\,32$, and $a \simeq 2.001\,27$ and $h_{\rm m} \simeq 1.000\,64$, respectively. Figure 7 shows contour plots of the velocity corresponding to the cases shown in Fig. 6; the contour interval is the same in both parts of the figure.

For small $N$ (typified by $N = 1/10$) two features of the flow are apparent. The first feature, evident in Fig. 7(a), is the formation of two regions with $h < 1$, adjacent to the contact lines,

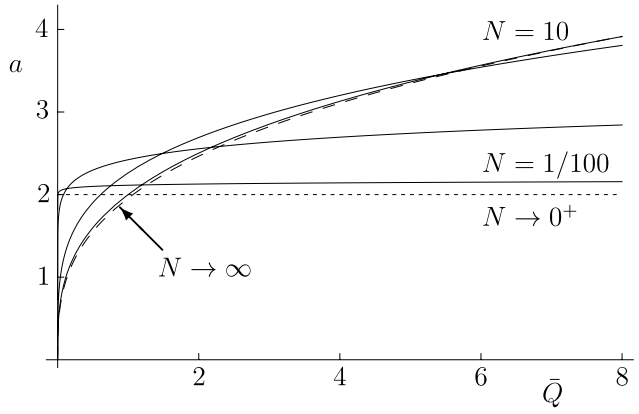


FIG. 5. Plot of the semi-width $a$ given by (29) as a function of $\bar{Q}$ in the special case of a vertical substrate ($\alpha = \pi/2$), for $N = 1/100$, $1/10$, 1, and 10. The dotted line shows the asymptotic solution $a = 2$ in the limit $N \to 0^+$, and the dashed line shows the asymptotic solution $a = (15\bar{Q}/2)^{1/3}$ in the limit $N \to \infty$.

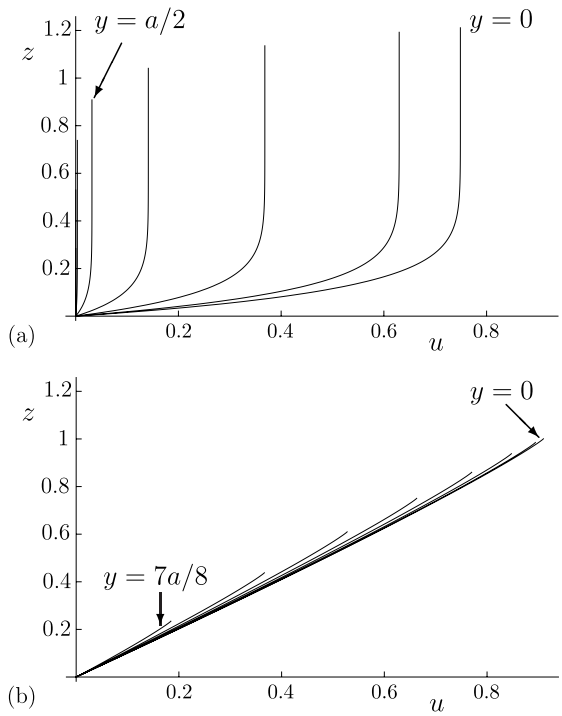


FIG. 6. Plots of the velocity profiles $u(y,z)$ given by (13) at positions $y = 0, a/8, a/4, \ldots, 7a/8$ across the rivulet in the special case of a vertical substrate ($\alpha = \pi/2$), for (a) $N = 1/10$ and (b) $N = 10$, with $\bar{Q} = 1$ in each case, for which (a) $a \simeq 2.422\,64$ and $h_{\rm m} \simeq 1.211\,32$, and (b) $a \simeq 2.001\,27$ and $h_{\rm m} \simeq 1.000\,64$.

in which $q$ is small and so $\mu$ is large, leading to a large viscous resistance, and hence almost stationary fluid. Thus the rivulet "self-channels" its flow down a narrow central channel of semi-width $\left[2N\log\left(\bar{Q}^2/4\pi N^3\right)\right]^{1/2}$ ($\ll 1$) between two "levées" of slowly moving fluid that form at its sides. These levées are reminiscent of the levées of unyielded (and hence stationary) fluid adjacent to the contact lines of rivulets of *viscoplastic* fluid reported by Wilson *et al.*[40] The second feature is that in the central channel, away from the substrate $z = 0$, the shear rate $q$ is small, and hence the viscosity $\mu$ is large; therefore, as is evident in Fig. 6(a), the velocity profiles have a "plug-like" form at each $y$ position, with most of the fluid moving with a velocity that is independent of $z$ but not of $y$. Specifically, $a \to 2^+$ and

$$u \sim Nh^{\frac{N+1}{N}} \sim \frac{\bar{Q}}{2\sqrt{\pi N}}\left(1-\frac{y^2}{4}\right)^{\frac{N+1}{N}} \quad \text{as} \quad N \to 0^+, \tag{30}$$

except in a narrow boundary layer near the substrate (where $u = 0$) in which the shear rate is large. As Fig. 7(a) illustrates, in this case there are relatively large velocity gradients in the $y$ direction in the middle of the rivulet (where the velocity is not small) as well as large velocity gradients in the $z$ direction near the substrate.

For large $N$ (typified by $N = 10$) the shear rate $q$ is uniform away from the free surface $z = h$ and the viscosity $\mu$ decreases linearly with $z$, and so, as is evident in Fig. 6(b), the velocity profile is linear in $z$. Specifically, $a \to (15\bar{Q}/2)^{1/3}$ and

$$q \to 1, \quad \mu \to h - z, \quad u \to z \quad \text{as} \quad N \to \infty, \tag{31}$$

except in a narrow boundary layer near the free surface (where $u_z = 0$) in which the gradient of shear is large. As Fig. 7(b) illustrates, in this case the velocity gradients are almost entirely in the $z$ direction over most of the rivulet.

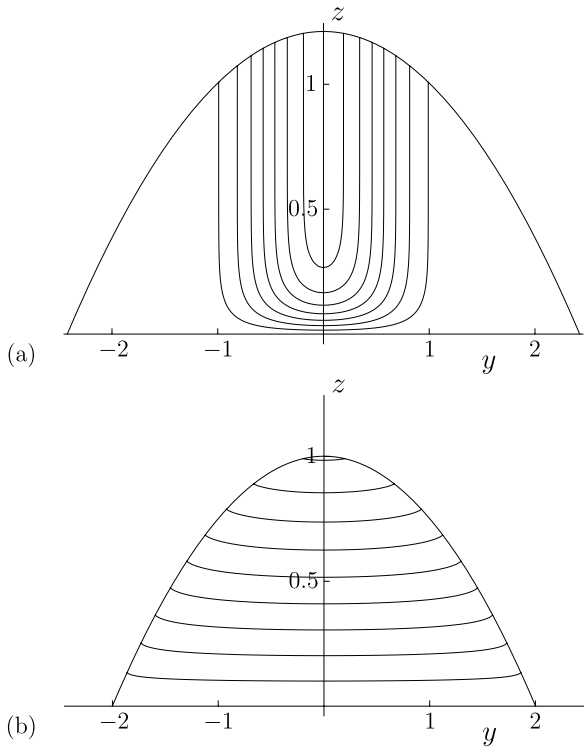


FIG. 7. Contour plots of the velocity $u(y,z)$ given by (13) in the special case of a vertical substrate ($\alpha = \pi/2$), for the same values of $N$ and $\bar{Q}$ as in Fig. 6, namely, (a) $N = 1/10$ and (b) $N = 10$, with $\bar{Q} = 1$ in each case. The contour interval is 0.1 in both parts of the figure.

Figure 8 shows a plot of the maximum velocity $u_{\max}$, namely,

$$u_{\max} = \frac{N}{N+1}\left(\frac{\bar{Q}}{4\,\mathrm{B}\left(\frac{3}{2},\frac{2N+1}{N}\right)}\right)^{\frac{N+1}{3N+1}}, \tag{32}$$

as a function of $N$ for different values of $\bar{Q}$ (and hence different values of $a$ and $h_{\mathrm{m}}$), showing that $u_{\max}$ decreases from $\infty$ (specifically, $u_{\max} \sim \bar{Q}(2\sqrt{\pi N})^{-1} \to \infty$ as $N \to 0^+$) to a minimum value, and then increases to $(15\bar{Q}/16)^{1/3}$ as $N \to \infty$, taking the value $u_{\max} = (105\bar{Q})^{1/2}/16$ when $N = 1$.

## IV. RIVULET FLOW DOWN A SLOWLY VARYING SUBSTRATE

### A. Flow around a large horizontal cylinder

Although the solution obtained in Subsection III B is for strictly unidirectional flow of a uniform rivulet of fluid of prescribed contact angle down a planar substrate, it also provides the leading order solution for *locally* unidirectional flow down a substrate whose inclination angle $\alpha$, rather than being constant, varies slowly in the downstream direction; the cross-sectional free surface profile of the rivulet (and in particular, the semi-width $a$ and maximum height $h_{\mathrm{m}}$) then varies slowly with position down the substrate. An example is provided by rivulet flow in the azimuthal direction around the outside of a large horizontal circular cylinder, the inclination angle $\alpha$ then varying slowly around the cylinder; in that case the flow corresponds to a prescribed flux of fluid being supplied at the top of the cylinder (where $\alpha = 0$), running around the cylinder under gravity, and falling off at the bottom (where $\alpha = \pi$). Figure 9 shows a sketch of such a situation; it is rivulet flow of this type that we describe in the remainder of the present work (although other interpretations are, of

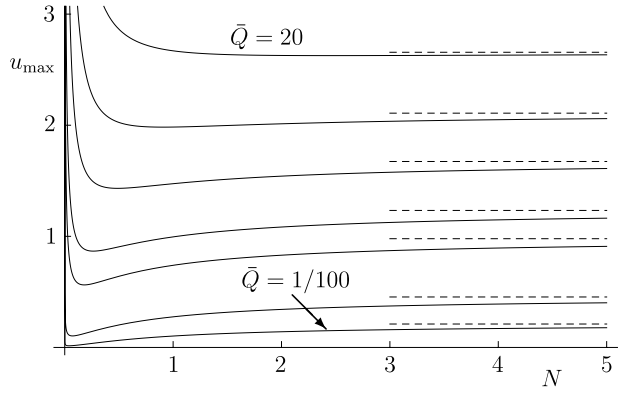


FIG. 8. Plot of the maximum velocity $u_{\max}$ given by (32) as a function of $N$ in the special case of a vertical substrate ($\alpha = \pi/2$), for $\bar{Q} = 1/100$, 1/10, 1, 2, 5, 10, and 20. The dashed lines show the asymptotic solution $u_{\max} = (15\bar{Q}/16)^{1/3}$ in the limit $N \to \infty$.

course, also possible). Specifically, we consider cases where the azimuthal aspect ratio $\epsilon = \ell/R$ and the appropriately defined reduced Reynolds number $Re^* = \rho\gamma\beta^4\ell^2/\bar{\mu}^2 R$, where $R$ is the radius of the cylinder, satisfy $\epsilon \ll \beta$ and $Re^* \ll 1$, the latter implying that inertial effects are negligible. In particular, both of these conditions are satisfied if $R$ is sufficiently large.

Figure 10 shows plots of (a) $a$ and (b) $h_{\rm m}$ as functions of $\alpha/\pi$ for various values of $N$; thus Fig. 10(a) shows half of the "footprint" of the rivulet on the cylinder, and Fig. 10(b) shows the profile of the centreline of the rivulet when the cylinder is viewed "end on" (both of them being "unwrapped" from the cylinder for the purposes of the figure).

Near the top of the cylinder, where the azimuthal component of gravity (proportional to $\sin\alpha$) driving the azimuthal flow is small but the normal component (proportional to $\cos\alpha$) tending to flatten the rivulet is significant, in order to achieve the prescribed flux $\bar{Q}$ the rivulet becomes wide and of finite thickness unity according to

$$a \sim \frac{(2N+1)\bar{Q}}{2N\alpha^{\frac{1}{N}}} \to \infty, \qquad h_{\rm m} \sim 1 + \frac{\alpha^2}{4} \to 1^+ \tag{33}$$

as $\alpha \to 0^+$. Near the bottom of the cylinder, where the azimuthal component of gravity is again small and the normal component, now tending to thicken the rivulet, is again significant, the rivulet

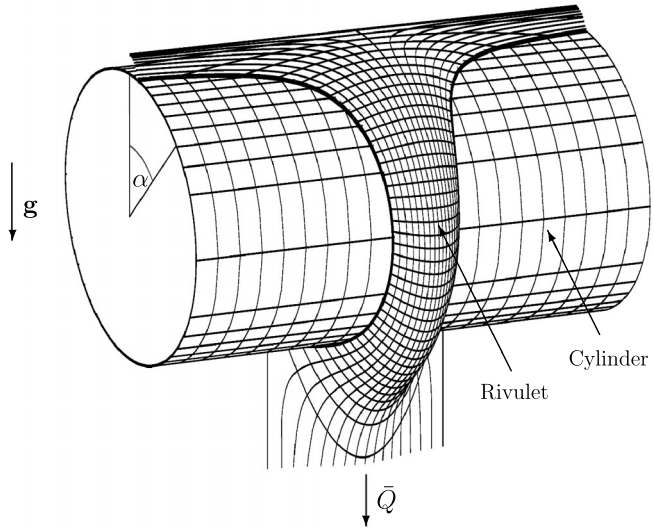


FIG. 9. Sketch of a slowly varying rivulet of prescribed flux $\bar{Q}$ with constant contact angle and slowly varying semi-width that runs from the top ($\alpha = 0$) to the bottom ($\alpha = \pi$) of a large horizontal circular cylinder.

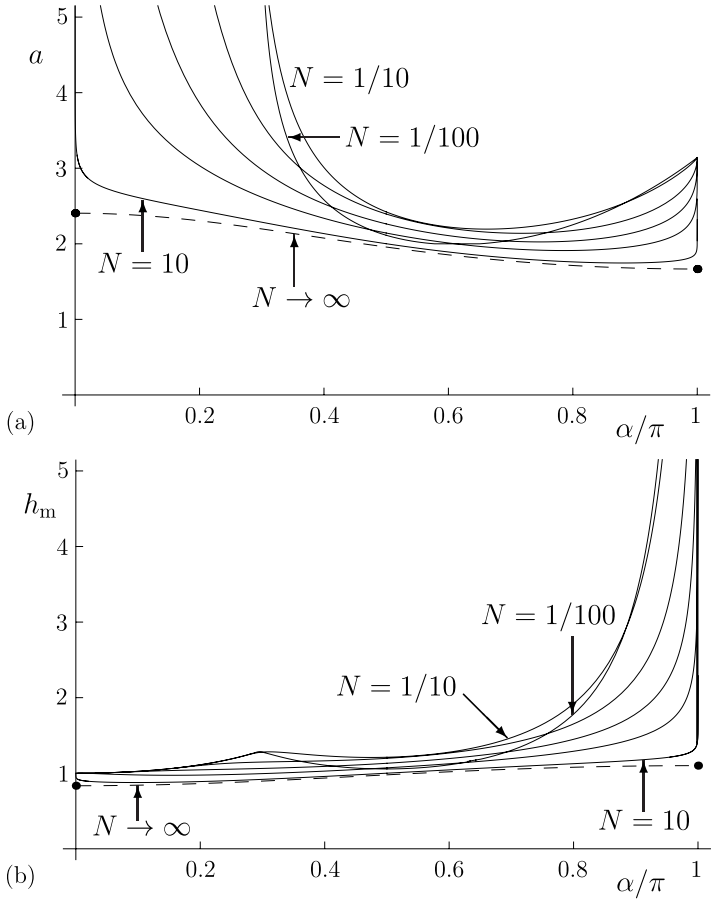


FIG. 10. Plots of (a) the semi-width $a$ and (b) the maximum thickness $h_\mathrm{m}$ as functions of $\alpha/\pi$ in the cases $N = 1/100$, $1/10$, $1/2$, 1, 2, and 10, for $\bar{Q} = 1$. The dashed curves show the leading order asymptotic outer solutions in the limit $N \to \infty$, and the dots denote the values $a \simeq 2.405\,15$ and $h_\mathrm{m} \simeq 0.834\,44$ at $\alpha = 0$ and $a \simeq 1.666\,39$ and $h_\mathrm{m} \simeq 1.100\,47$ at $\alpha = \pi$ on these asymptotic solutions.

becomes thick and of finite width $\pi$ according to

$$a \sim \pi - \frac{2}{\kappa_N}\left(\frac{\pi-\alpha}{\bar{Q}^N}\right)^{\frac{1}{2N+1}} \to \pi^-, \qquad h_\mathrm{m} \sim \kappa_N\left(\frac{\bar{Q}^N}{\pi-\alpha}\right)^{\frac{1}{2N+1}} \to \infty \tag{34}$$

as $\alpha \to \pi^-$; therefore the thin-film approximation will break down sufficiently near to $\alpha = \pi$. At the middle of the cylinder ($\alpha = \pi/2$), where the azimuthal component of gravity is significant but the normal component is zero, the rivulet has finite width and thickness given by (29).

As Fig. 10(a) shows, the rivulet narrows to a minimum width and then widens again as it flows around the cylinder. Its minimum width occurs on the lower half of the cylinder ($\pi/2 < \alpha < \pi$), at a position determined mathematically by (17) and

$$2\csc^2\alpha = N\,\frac{f_N'(ma)ma}{f_N(ma)} - 3N + 1, \tag{35}$$

the latter obtained by differentiation of (17) with respect to $\alpha$, with $Q = \bar{Q}$; it may be shown from (17) and (35) that $a$ has a (unique) stationary point for all values of $N$ and $\bar{Q}$.

On the other hand, as Fig. 10(b) shows, the nature of the stationary points of $h_\mathrm{m}$, determined mathematically by (17) and

$$2\csc^2\alpha = N\,\frac{f_N'(ma)\sinh ma}{f_N(ma)} - 3N + 1, \tag{36}$$

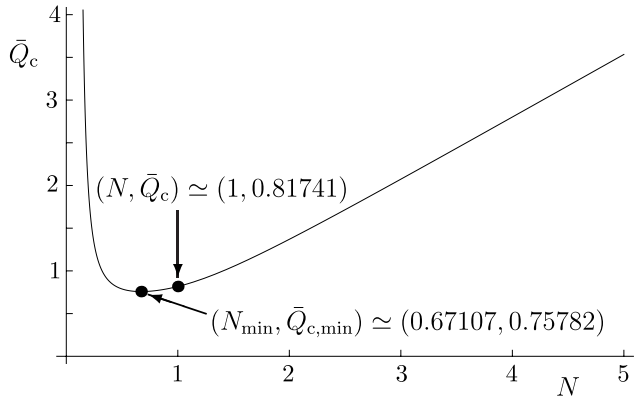


FIG. 11. Plot of the critical flux $\bar{Q}_c$ as a function of $N$. The dots denote the minimum value $\bar{Q}_c = \bar{Q}_{c,min} \simeq 0.757\,82$ at $N = N_{min} \simeq 0.671\,07$ and the Newtonian value $\bar{Q}_c \simeq 0.817\,41$ at $N = 1$.

the latter obtained by differentiation of (12) and (17) with respect to $\alpha$, depends on the value of $\bar{Q}$. Specifically, it may be shown from (17) and (36) that there exists a critical ($N$-dependent) flux $\bar{Q} = \bar{Q}_c(N)$ such that if $\bar{Q} < \bar{Q}_c$ then $h_m$ has two stationary points, and increases from $h_m = 1$ at $\alpha = 0$ to a maximum in $0 < \alpha < \pi/2$, decreases to a minimum also in $0 < \alpha < \pi/2$, and then increases monotonically to infinity as $\alpha \to \pi^-$, whereas if $\bar{Q} \geq \bar{Q}_c$ then $h_m$ has no stationary points, and increases monotonically from $h_m = 1$ at $\alpha = 0$ to $\infty$ as $\alpha \to \pi^-$. Figure 11 shows a plot of $\bar{Q}_c$ as a function of $N$, showing that $\bar{Q}_c$ decreases from $\infty$ as $N \to 0^+$ to a minimum value $\bar{Q}_c = \bar{Q}_{c,min} \simeq 0.757\,82$ at $N = N_{min} \simeq 0.671\,07$, and then increases to $\infty$ as $N \to \infty$, taking the value $\bar{Q}_c \simeq 0.817\,41$ when $N = 1$. Note also from Fig. 11 that if $\bar{Q} \leq \bar{Q}_{c,min}$ then $h_m$ has two stationary points for any $N$, whereas if $\bar{Q} > \bar{Q}_{c,min}$ then $h_m$ has two stationary points only if $N$ is either sufficiently small or sufficiently large.

As Fig. 10 also shows, $a$ and $h_m$ vary non-monotonically with $N$, in the sense that at any fixed value of $\alpha$, both $a$ and $h_m$ increase with $N$ up to a maximum and then decrease monotonically.

Figure 10 also includes (as dashed curves) the leading order asymptotic outer solutions (away from $\alpha = 0$ and $\alpha = \pi$) for $a$ and $h_m$ in the limit $N \to \infty$, obtained by solving (27) with $Q = \bar{Q}$ for $a$ and then using (12) for $h_m$. In particular, Fig. 10 shows that these outer solutions take finite values at the top and bottom of the cylinder, namely, $a \simeq 2.405\,15$ and $h_m \simeq 0.834\,44$ at $\alpha = 0$, and $a \simeq 1.666\,39$ and $h_m \simeq 1.100\,47$ at $\alpha = \pi$, obtained by solving $\bar{Q} = f_\infty(a)/9$. When $N$ is large but finite, there is a thin boundary layer near $\alpha = 0$ in which the solution for $a$ grows without bound and the solution for $h_m$ adjusts to the value $h_m = 1$ given by (33) at $\alpha = 0$, and a thin boundary layer near $\alpha = \pi$ in which the solution for $h_m$ grows without bound and the solution for $a$ adjusts to the value $a = \pi$ given by (34) at $\alpha = \pi$.

In the limit $N \to 0^+$ the positions of the minimum of $a$ and of the maximum and minimum of $h_m$ approach $\alpha = \pi/2$, while in the limit $N \to \infty$ the position of the minimum of $a$ approaches $\alpha = \pi$ and the positions of the maximum and minimum of $h_m$ approach $\alpha = 0$.

### B. Free surface profiles *h*

Figure 12 shows plots of the cross-sectional free surface profile $h$ as a function of $y$ at the stations $\alpha = \pi/20, \pi/10, \ldots, 19\pi/20$ around the cylinder, for $N = 1/2$ and $\bar{Q} = 1$, and Figure 13 shows corresponding plots for $N = 2$. As already described, the profiles are wide and of finite thickness near the top of the cylinder, but are thick and of finite width near the bottom of the cylinder. The non-monotonic variation of $a$ with $\alpha$ is evident in part (b) of both figures. Figure 12 shows a case for which $\bar{Q} = 1 > \bar{Q}_c(1/2) \simeq 0.788\,18$, and so $h_m$ increases monotonically with $\alpha$ in this case, whereas Fig. 13 shows a case for which $\bar{Q} = 1 < \bar{Q}_c(2) \simeq 1.369\,80$, and so $h_m$ varies non-monotonically with $\alpha$, having a local maximum and a local minimum (both of which are barely discernible in the figure) on the upper half of the cylinder in this case.

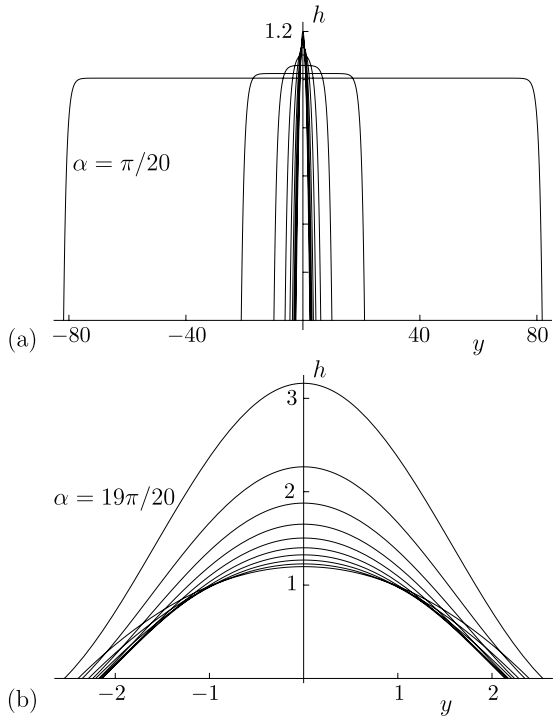


FIG. 12. Plot of the cross-sectional free surface profile $h$ given by (11) as a function of $y$ at the stations (a) $\alpha = \pi/20, \pi/10, \ldots, \pi/2$ on the upper half of cylinder, and (b) $\alpha = \pi/2, 11\pi/20, \ldots, 19\pi/20$ on the lower half of cylinder, for $N = 1/2$ and $\bar{Q} = 1$. Note the different scales used on the axes in the two parts of the figure.

Figure 14 shows contour plots of the free surface profile $h$ in the $(y, \alpha/\pi)$ plane, for several values of $N$, for $\bar{Q} = 1$. The non-monotonic variation of $a$ with $\alpha$, evident in all of the cases shown in Fig. 14, is qualitatively the same for all values of $\bar{Q}$. On the other hand, the form of the variation of $h$ with $\alpha$ depends on $\bar{Q}$. In particular, since at each station $\alpha$, $h$ has a maximum $h_m$ at $y = 0$, if $\bar{Q} < \bar{Q}_c$ then the maximum of $h_m$ (regarded as a function of $\alpha$) that occurs corresponds to a local maximum of $h$ (regarded as a function of $\alpha$ and $y$), whereas the minimum of $h_m$ corresponds to a saddle point of $h$; if $\bar{Q} \geq \bar{Q}_c$ then $h_m$ has no stationary points and so $h$ has no stationary points. Figures 14(a) and 14(c) are for cases with $\bar{Q} = 1 < \bar{Q}_c(1/5) \simeq 1.918\,57$ and $\bar{Q} = 1 < \bar{Q}_c(2) \simeq 1.369\,80$, respectively, so that $h_m$ has a local maximum and minimum, and therefore $h$ has a local maximum and a saddle point, at $(y, \alpha/\pi, h_m) \simeq (0, 0.300\,00, 1.243\,13)$ and $(y, \alpha/\pi, h_m) \simeq (0, 0.440\,11, 1.227\,39)$ in (a), and at $(y, \alpha/\pi, h_m) \simeq (0, 0.005\,82, 1.000\,05)$ (very close to the top of the cylinder) and $(y, \alpha/\pi, h_m) \simeq (0, 0.154\,36, 0.972\,88)$ in (c), all of which are marked with dots; the contour that passes through the saddle point of $h$ is also included in each case. Part (d) shows an enlargement of (c) (with additional contours, shown dashed and dotted) near the top of the cylinder, illustrating more clearly the occurrence of a local maximum in $h$ there. Figure 14(b) is for a case with $\bar{Q} = 1 > \bar{Q}_c(1) \simeq 0.817\,41$, and so $h$ has no stationary points; an additional contour $h = 1.01$ is included (shown dashed) to illustrate the general form of the contours near the top of the cylinder. In all cases, since $h_m \to \infty$ in the limit $\alpha \to \pi^-$, there should, in principle, be infinitely many contours near the bottom of the cylinder, but only contours up to $h = 8$ are plotted. Note also that near the top of the cylinder in Fig. 14(a) the rivulet is wide and the free surface profile is relatively flat (that is, $h$ varies only slowly with $\alpha/\pi$ and with $y$ away from the contact lines, as in Fig. 12(a)), explaining why there are so few contours there.

Velocity profiles and contours of the velocity in cross sections of the rivulet at different $\alpha$, as well as the maximum velocity $u_{max}$, are qualitatively similar to those in the case $\alpha = \pi/2$ shown in Figs. 6–8, and so, for brevity, are not reproduced here.

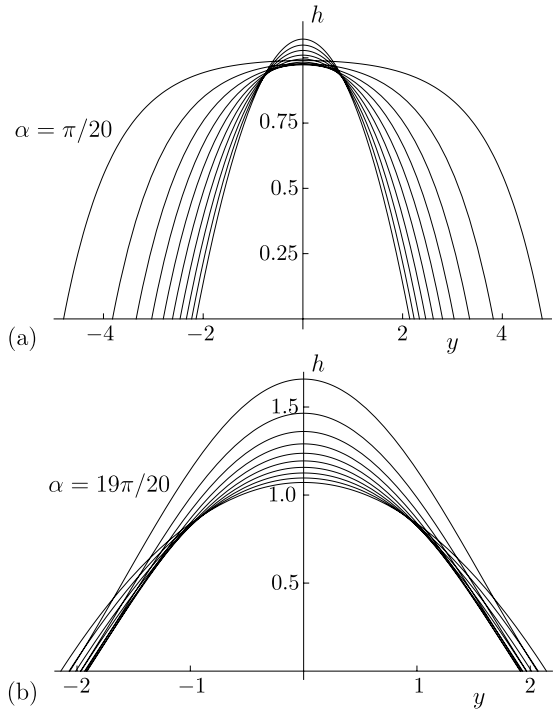


FIG. 13. As in Fig. 12, except for $N = 2$.

### C. The limits of small and large flux $\bar{Q}$

In the limit of small flux, $\bar{Q} \to 0^+$, the rivulet becomes narrow and shallow according to

$$a \sim 2h_{\mathrm{m}} \sim 2\left(\frac{9^N \bar{Q}^N}{\lambda_N^N \sin\alpha}\right)^{\frac{1}{3N+1}} = O\left(\bar{Q}^{\frac{N}{3N+1}}\right) \to 0^+; \tag{37}$$

also the position of the minimum of $a$ approaches $\alpha = \pi/2^+$, and the positions of the maximum and minimum of $h_{\mathrm{m}}$ approach $\alpha = 0$ and $\alpha = \pi/2^-$, respectively.

In the limit of large flux, $\bar{Q} \to \infty$, the rivulet becomes infinitely wide on the upper half of the cylinder and infinitely thick on the lower half of the cylinder according to

$$a \sim \frac{(2N+1)\bar{Q}}{2N}\left(\frac{m^{2N+1}}{\sin\alpha}\right)^{\frac{1}{N}} = O\left(\bar{Q}\right) \to \infty, \qquad h_{\mathrm{m}} \to \frac{1}{m} = O(1) \tag{38}$$

for $0 < \alpha < \pi/2$,

$$a = 2h_{\mathrm{m}} = 2\left(\frac{9\bar{Q}}{\lambda_N}\right)^{\frac{N}{3N+1}} = O\left(\bar{Q}^{\frac{N}{3N+1}}\right) \to \infty \tag{39}$$

at $\alpha = \pi/2$, and

$$a \to \frac{\pi}{m} = O(1), \qquad h_{\mathrm{m}} \sim \kappa_N\left(\frac{m^N \bar{Q}^N}{\sin\alpha}\right)^{\frac{1}{2N+1}} = O\left(\bar{Q}^{\frac{N}{2N+1}}\right) \to \infty \tag{40}$$

for $\pi/2 < \alpha < \pi$; also the position of the minimum of $a$ approaches $\alpha = \pi^-$.

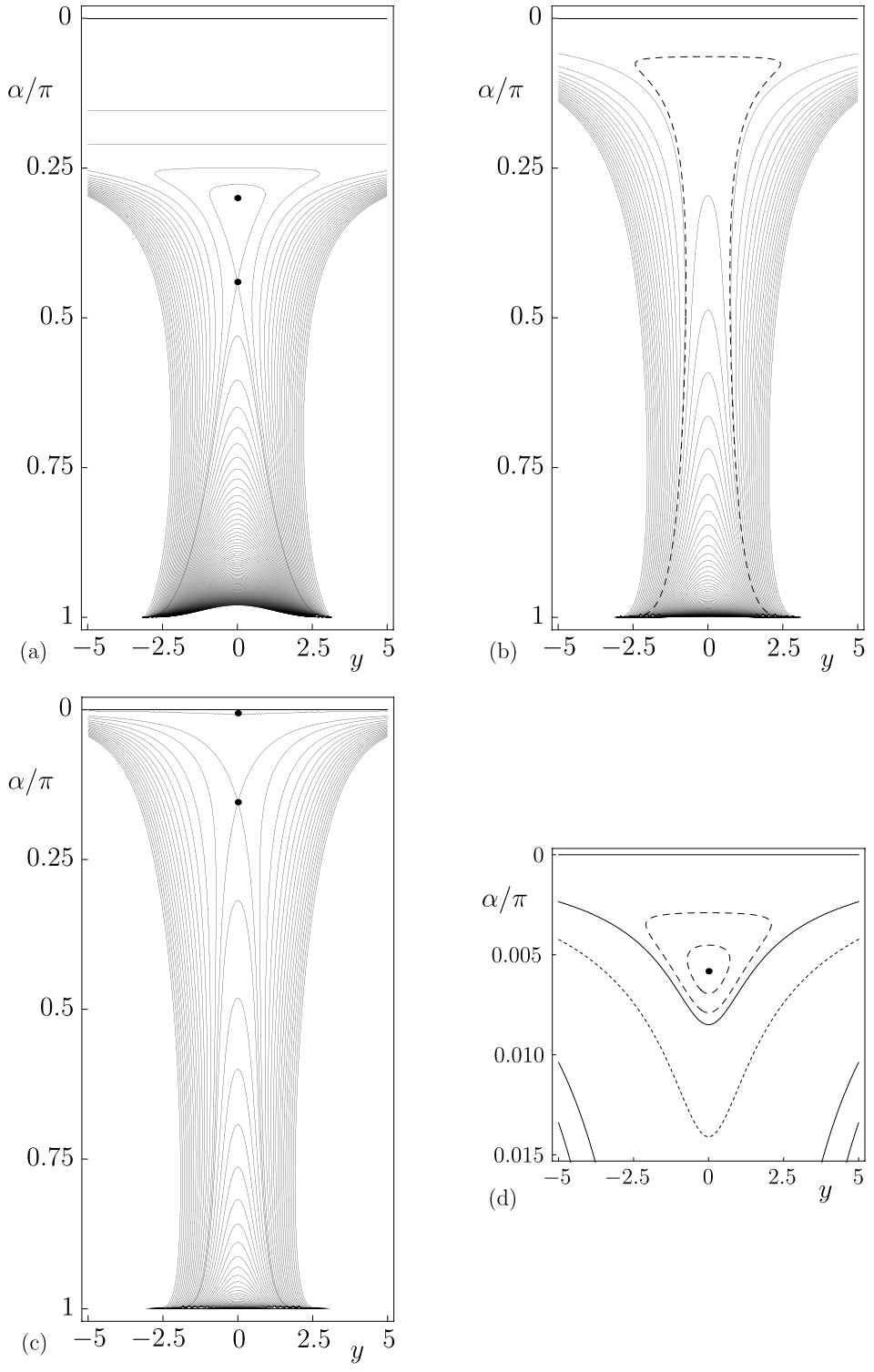


FIG. 14. Contour plots of the free surface profile $h$ in the $(y, \alpha/\pi)$ plane in the cases (a) $N = 1/5$, (b) $N = 1$, and (c) $N = 2$, for $\bar{Q} = 1$. In each case the contours are drawn at intervals of $1/16$, up to a maximum $h = 8$. The local maximum and the saddle point of $h$, at $(y, \alpha/\pi, h_{\mathrm{m}}) \simeq (0, 0.300\,00, 1.243\,13)$ and $(y, \alpha/\pi, h_{\mathrm{m}}) \simeq (0, 0.440\,11, 1.227\,39)$ in (a), and at $(y, \alpha/\pi, h_{\mathrm{m}}) \simeq (0, 0.005\,82, 1.000\,05)$ and $(y, \alpha/\pi, h_{\mathrm{m}}) \simeq (0, 0.154\,36, 0.972\,88)$ in (c), are marked with dots, and the contour that passes through the saddle point is also included. Part (d) shows an enlargement of (c) near the top of the cylinder, with additional contours $h = 1.000\,02$ and $h = 1.000\,04$ (shown dashed) and $h = 0.9995$ (shown dotted). In (b), $h$ has no stationary points; an additional contour $h = 1.01$ is included (shown dashed).

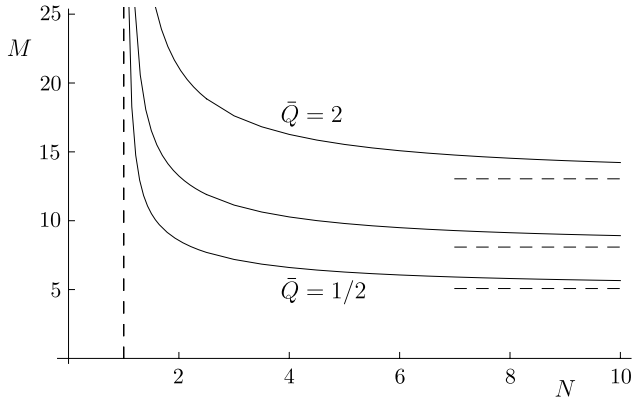


FIG. 15. Plot of the mass of the rivulet, $M$, given by (41) as a function of $N$, in the cases $\bar{Q} = 1/2$, 1, and 2. The horizontal dashed lines show the constant asymptotic values in the limit $N \to \infty$. The vertical dashed line shows the value $N = 1$, at and below which the mass is infinite.

### D. The mass of the rivulet, *M*

The mass of the rivulet, denoted by $M$ and non-dimensionalised with $\rho\beta\ell^2 R$, is given by

$$M = \int_0^{\pi}\int_{-a}^{a} h\,\mathrm{d}y\,\mathrm{d}\alpha = \int_0^{\frac{\pi}{2}} \frac{2(ma\coth ma - 1)}{m^2}\,\mathrm{d}\alpha + \int_{\frac{\pi}{2}}^{\pi} \frac{2(1 - ma\cot ma)}{m^2}\,\mathrm{d}\alpha. \tag{41}$$

Both of the integrands in (41) are finite at $\alpha = \pi/2$. The second integrand is singular like $O((\pi - \alpha)^{-1/(2N+1)})$ as $\alpha \to \pi^-$ (i.e., near the bottom of the cylinder) and hence is integrable there; however, the first integrand is singular like $O(\alpha^{-1/N})$ as $\alpha \to 0^+$ (i.e., near the top of the cylinder) and so this integral is divergent if $N \le 1$ but is convergent if $N > 1$, showing that the mass is theoretically infinite in the Newtonian case $N = 1$ and in the shear-thinning case $N < 1$, but that it is finite in the shear-thickening case $N > 1$. In other words, the finite mass in the case $N > 1$ is due to the slower divergence of the width of the rivulet at the top of the cylinder than in the case $N \le 1$. Figure 15 shows a plot of $M$ as a function of $N$ for various values of $\bar{Q}$, confirming this behaviour and showing that $M$ decreases monotonically from $\infty$ to a (nonzero) $\bar{Q}$-dependent constant asymptotic value (determined by (17), (28), and (41)) in the limit $N \to \infty$.

## V. CONCLUSIONS

In order to begin to rectify the lack of understanding of non-Newtonian rivulet flow, we considered locally unidirectional steady gravity-driven flow of a thin rivulet of a power-law fluid with prescribed volume flux $\bar{Q}$ down a locally planar substrate. In Sec. III B we obtained the solution for unidirectional flow of a uniform rivulet down a planar substrate, and then in Sec. IV we used it to obtain the solution for a slowly varying rivulet with prescribed constant (nonzero) contact angle $\beta$ down a slowly varying substrate, specifically flow in the azimuthal direction around the outside of a large horizontal circular cylinder.

As in the special case of a Newtonian fluid, the rivulet is always wide and of finite thickness near the top of the cylinder, but is thick and of finite width near the bottom of the cylinder. In addition, the minimum width of the rivulet always occurs on the lower half of the cylinder, whereas the maximum thickness $h_{\mathrm{m}}$ either increases monotonically with the angle $\alpha$ measured around the cylinder (if $\bar{Q} \ge \bar{Q}_{\mathrm{c}}$), or it has a maximum and then a minimum on the upper half of the cylinder (if $\bar{Q} < \bar{Q}_{\mathrm{c}}$).

The solution was shown to depend strongly on the value of the power-law index of the fluid. For example, as Figs. 6(a) and 7(a) illustrate, a rivulet of strongly shear-thinning fluid self-channels its flow down a narrow central channel between two levées of slowly moving fluid that form at its sides, and in the central channel there is a plug-like flow at each $y$ position except in a boundary

layer near the substrate. On the other hand, as Figs. 6(b) and 7(b) illustrate, in a rivulet of a strongly shear-thickening fluid the velocity profile is linear in $z$ except in a boundary layer near the free surface. Another notable qualitative departure from Newtonian behaviour is that, as Fig. 15 shows, whereas the mass of a rivulet of a Newtonian or a shear-thinning fluid is theoretically infinite, the mass of a rivulet of a shear-thickening fluid is finite.

In the present work we have compared rivulets with the same or different values of the dimensionless prescribed flux $\bar{Q}$. Since the scaling of the volume flux in (8) involves $N$, a prescribed value of $\bar{Q}$ would, in general, correspond to different values of the dimensional prescribed flux for different fluids (i.e., for different values of $N$). However, solutions for rivulets of different power-law fluids with the same prescribed value of the dimensional flux may readily be obtained from the present solution once the values of the parameters $\rho$, $\mu_N$, $\gamma$, and $\beta$ for the different fluids are specified.

As well as being of interest in its own right, the present results provide a benchmark for the study of rivulet flow of more realistic (and hence more mathematically complicated) non-Newtonian fluids.

## ACKNOWLEDGMENTS

The first author (F.H.H.A.) wishes to thank the Ministry of Education, Kingdom of Saudi Arabia and King Faisal University for financial support via an Academic Staff Training Fellowship. The third author (S.K.W.) is supported by Leverhulme Trust Research Fellowship RF-2013-355 "Small Particles, Big Problems: Understanding the Complex Behaviour of Nanofluids."

[1] G. Ribatski and A. M. Jacobi, "Falling-film evaporation on horizontal tubes-a critical review," Int. J. Refrig. **28**, 635–653 (2005).
[2] N. J. Balmforth, R. V. Craster, and R. Sassi, "Shallow viscoplastic flow on an inclined plane," J. Fluid Mech. **470**, 1–29 (2002).
[3] C. Lemaitre, E. de Langre, and P. Hémon, "Rainwater rivulets running on a stay cable subject to wind," Eur. J. Mech. - B/Fluids **29**, 251–258 (2010).
[4] A. C. Robertson, I. J. Taylor, S. K. Wilson, B. R. Duffy, and J. M. Sullivan, "Numerical simulation of rivulet evolution on a horizontal cable subject to an external aerodynamic field," J. Fluids Struct. **26**, 50–73 (2010).
[5] M. E. Labib, S. Dukhin, J. Murawski, Y. Tabani, and R. Lai, "Surfactant influence on rivulet droplet flow in minitubes and capillaries and its downstream evolution," Adv. Colloid Interface Sci. **166**, 60–86 (2011).
[6] G. D. Towell and L. B. Rothfeld, "Hydrodynamics of rivulet flow," AIChE J. **12**, 972–980 (1966).
[7] R. F. Allen and C. M. Biggin, "Longitudinal flow of a lenticular liquid filament down an inclined plane," Phys. Fluids **17**, 287–291 (1974).
[8] B. R. Duffy and H. K. Moffatt, "Flow of a viscous trickle on a slowly varying incline," Chem. Eng. J. **60**, 141–146 (1995).
[9] P. A. Kuibin, "An asymptotic description of the rivulet flow along an inclined cylinder," Russ. J. Eng. Thermophys. **6**, 33–45 (1996).
[10] S. V. Alekseenko, P. I. Geshev, and P. A. Kuibin, "Free-boundary fluid flow on an inclined cylinder," Phys.-Dokl. **42**, 269–272 (1997).
[11] S. K. Wilson and B. R. Duffy, "A rivulet of perfectly wetting fluid draining steadily down a slowly varying substrate," IMA J. Appl. Math. **70**, 293–322 (2005).
[12] A. J. Tanasijczuk, C. A. Perazzo, and J. Gratton, "Navier–Stokes solutions for steady parallel-sided pendent rivulets," Eur. J. Mech. - B/Fluids **29**, 465–471 (2010).
[13] D. Holland, B. R. Duffy, and S. K. Wilson, "Thermocapillary effects on a thin viscous rivulet draining steadily down a uniformly heated or cooled slowly varying substrate," J. Fluid Mech. **441**, 195–221 (2001).
[14] S. K. Wilson and B. R. Duffy, "Strong temperature-dependent-viscosity effects on a rivulet draining down a uniformly heated or cooled slowly varying substrate," Phys. Fluids **15**, 827–840 (2003).
[15] T. G. Myers, H. X. Liang, and B. Wetton, "The stability and flow of a rivulet driven by interfacial shear and gravity," Int. J. Nonlinear Mech. **39**, 1239–1249 (2004).
[16] S. K. Wilson and B. R. Duffy, "Unidirectional flow of a thin rivulet on a vertical substrate subject to a prescribed uniform shear stress at its free surface," Phys. Fluids **17**, 108105 (2005).
[17] J. M. Sullivan, C. Paterson, S. K. Wilson, and B. R. Duffy, "A thin rivulet or ridge subject to a uniform transverse shear stress at its free surface due to an external airflow," Phys. Fluids **24**, 082109 (2012).
[18] C. Paterson, S. K. Wilson, and B. R. Duffy, "Rivulet flow round a horizontal cylinder subject to a uniform surface shear stress," Q. J. Mech. Appl. Math. **67**, 567–597 (2014).
[19] C. Paterson, S. K. Wilson, and B. R. Duffy, "Pinning, de-pinning and re-pinning of a slowly varying rivulet," Eur. J. Mech. - B/Fluids **41**, 94–108 (2013).
[20] P. C. Smith, "A similarity solution for slow viscous flow down an inclined plane," J. Fluid Mech. **58**, 275–288 (1973).
[21] B. R. Duffy and H. K. Moffatt, "A similarity solution for viscous source flow on a vertical plane," Eur. J. Appl. Math. **8**, 37–47 (1997).

[22] Y. M. Yatim, B. R. Duffy, S. K. Wilson, and R. Hunt, "Similarity solutions for unsteady gravity-driven slender rivulets," Q. J. Mech. Appl. Math. **64**, 455–480 (2011).
[23] G. W. Young and S. H. Davis, "Rivulet instabilities," J. Fluid Mech. **176**, 1–31 (1987).
[24] P. Schmuki and M. Laso, "On the stability of rivulet flow," J. Fluid Mech. **215**, 125–143 (1990).
[25] E. S. Benilov, "On the stability of shallow rivulets," J. Fluid Mech. **636**, 455–474 (2009).
[26] J. A. Diez, A. G. González, and L. Kondic, "On the breakup of fluid rivulets," Phys. Fluids **21**, 082105 (2009).
[27] J. A. Diez, A. G. González, and L. Kondic, "Instability of a transverse liquid rivulet on an inclined plane," Phys. Fluids **24**, 032104 (2012).
[28] S. K. Wilson, J. M. Sullivan, and B. R. Duffy, "The energetics of the breakup of a sheet and of a rivulet on a vertical substrate in the presence of a uniform surface shear stress," J. Fluid Mech. **674**, 281–306 (2011).
[29] M. A. Herrada, A. S. Mohamed, J. M. Montanero, and A. M. Gañán-Calvo, "Stability of a rivulet flowing in a microchannel," Int. J. Multiphase Flow **69**, 1–7 (2015).
[30] S. V. Alekseenko, D. M. Markovich, and S. I. Shtork, "Wave flow of rivulets on the outer surface of an inclined cylinder," Phys. Fluids **8**, 3288–3299 (1996).
[31] S. V. Alekseenko, A. V. Bobylev, and D. M. Markovich, "Rivulet flow on the outer surface of an inclined cylinder," J. Eng. Thermophys. **17**, 259–272 (2008).
[32] S. V. Alekseenko, A. V. Bobylev, V. V. Guzanov, D. M. Markovich, and S. M. Kharlamov, "Regular waves on vertical falling rivulets at different wetting contact angles," Thermophys. Aeromech. **17**, 345–357 (2010).
[33] A. V. Bobylev, D. M. Markovich, and S. M. Kharlamov, "Investigation of the velocity field in the wave rivulet flowing down a vertical plate," Interfacial Phenom. Heat Transfer **2**, 119–127 (2014).
[34] T. Nakagawa and J. C. Scott, "Stream meanders on a smooth hydrophobic surface," J. Fluid Mech. **149**, 89–99 (1984).
[35] H.-Y. Kim, J.-H. Kim, and B. H. Kang, "Meandering instability of a rivulet," J. Fluid Mech. **498**, 245–256 (2004).
[36] K. Mertens, V. Putkaradze, and P. Vorobieff, "Morphology of a stream flowing down an inclined plane. Part 1. Braiding," J. Fluid Mech. **531**, 49–58 (2005).
[37] B. Birnir, K. Mertens, V. Putkaradze, and P. Vorobieff, "Morphology of a stream flowing down an inclined plane. Part 2. Meandering," J. Fluid Mech. **607**, 401–411 (2008).
[38] A. Daerr, J. Eggers, L. Limat, and N. Valade, "General mechanism for the meandering instability of rivulets of Newtonian fluids," Phys. Rev. Lett. **106**, 184501 (2011).
[39] S. Rosenblat, "Rivulet flow of a viscoelastic liquid," J. Non-Newtonian Fluid Mech. **13**, 259–277 (1983).
[40] S. K. Wilson, B. R. Duffy, and A. B. Ross, "On the gravity-driven draining of a rivulet of a viscoplastic material down a slowly varying substrate," Phys. Fluids **14**, 555–571 (2002).
[41] S. D. R. Wilson and S. L. Burgess, "The steady, spreading flow of a rivulet of mud," J. Non-Newtonian Fluid Mech. **79**, 77–85 (1998).
[42] S. K. Wilson, B. R. Duffy, and R. Hunt, "A slender rivulet of a power-law fluid driven by either gravity or a constant shear stress at the free surface," Q. J. Mech. Appl. Math. **55**, 385–408 (2002).
[43] Y. M. Yatim, S. K. Wilson, and B. R. Duffy, "Unsteady gravity-driven slender rivulets of a power-law fluid," J. Non-Newtonian Fluid Mech. **165**, 1423–1430 (2010).
[44] T. G. Myers, "Application of non-Newtonian models to thin film flow," Phys. Rev. E **72**, 066302 (2005).
[45] H. A. Barnes, J. F. Hutton, and K. Walters, *An Introduction to Rheology* (Elsevier, Amsterdam, 1989).